

Simulating Complex Fracture Systems in Geothermal Reservoirs Using an Explicitly Coupled Hydro-Geomechanical Model

Fu, P., Johnson, S.M. and Carrigan, C.R.

Lawrence Livermore National Laboratory, Livermore, CA, U.S.A.

Copyright 2011 ARMA, American Rock Mechanics Association

This paper was prepared for presentation at the 45th US Rock Mechanics / Geomechanics Symposium held in San Francisco, CA, June 26–29, 2011.

This paper was selected for presentation at the symposium by an ARMA Technical Program Committee based on a technical and critical review of the paper by a minimum of two technical reviewers. The material, as presented, does not necessarily reflect any position of ARMA, its officers, or members. Electronic reproduction, distribution, or storage of any part of this paper for commercial purposes without the written consent of ARMA is prohibited. Permission to reproduce in print is restricted to an abstract of not more than 300 words; illustrations may not be copied. The abstract must contain conspicuous acknowledgement of where and by whom the paper was presented.

ABSTRACT: Low permeability geothermal reservoirs can be stimulated by hydraulic fracturing to create Enhanced (or Engineered) Geothermal Systems (EGS) with higher permeability and improved heat transfer to increase heat production. Most existing analytical and numerical models for hydraulic fracturing focus on the propagation of a single fracture in the rock matrix whereas real hydraulic fracturing processes usually involve complex interactions between multiple fractures. In this paper, we document our effort to develop a numerical simulator with explicit geomechanics-discrete flow network coupling by utilizing and further advancing the simulation capabilities of the Livermore Distinct Element Code (LDEC). We describe the important modules of the simulator in the paper: an explicit finite element solid solver, a finite volume method flow solver, a joint model using the combined FEM-DEM capability of LDEC, and an adaptive remeshing module. The numerical implementation is verified against the classical KGD model. The interaction between two fractures with simple geometry and the stimulation of a relatively complex existing fracture network under different in-situ stress conditions are studied with the simulator.

1. INTRODUCTION

Engineered geothermal systems are created mainly through stimulation of lower permeability target formations using hydraulic fracturing to create or improve the subsurface heat exchanger component [1]. As a prerequisite to the successful enhancement of permeability between the injection wells and the production wells, both the MIT study [1] and DOE GTP panel express the need for guidance provided by credible hydraulic-fracturing stimulation models capable of addressing the propagation of clusters of fractures in hard rock.

While hydraulic fracturing has been in use for decades [2], understanding relatively complex fracture systems consisting of both pre-existing and newly created (by hydraulic stimulation) fractures remains a challenging task. A thorough review of the development of computer simulation techniques for hydraulic fracturing was provided by Adachi et al.[3] and thus is not repeated here. Among the existing models/methods, the classic PKN and KGD models [4-7] only handle the propagation of a single fracture with assumed simple geometries in a homogeneous medium. The pseudo-3D (P3D) and planar 3D (PL3D) models [3] are capable of

simulating fractures vertically extending through multiple geologic layers, but each simulation can only handle one crack lying in a single vertical plane. Although a number of models have emerged in recent years to explicitly simulate discrete fracture networks (e.g.[8]), the key mechanisms governing the interactions between the propagating new fractures and the existing fracture network, and the coupling between geomechanics and fluid dynamics, have not been rigorously included.

The principal objective of this work is to develop realistic computer-based models of EGS stimulation-response scenarios involving hydraulic stimulation of fracture systems in hard rock formations where a pre-existing fracture network may be present along with regional stress and temperature distributions. Our proposed approach is intended to assess the influence of many of the pertinent effects for EGS (e.g., formation mechanical characteristics, initial thermal and stress state of formation, hydraulic pumping parameters, etc.) on the time-dependent heat transfer capability of an initially low-permeability target formation. While much attention in the literature has been paid to exploring the local effects of stimulation near a single well bore, we aim to investigate how the stimulation of multiple wells,

spaced across the reservoir, will influence heat transfer on a reservoir scale by enhancing formation connectivity and permeability subject to realistic thermal and regional stress conditions. The ultimate goal of our work is to provide insight into selecting the best choices for producing long-term permeability enhancement on a site-by-site basis. This paper summarizes our initial research effort up to date, focusing on the development of numerical methods to simulate hydraulic fracturing and the preliminary findings.

2. GENERAL APPROACH

A real hydraulic fracturing process involves complex interactions between multiple fractures: New fractures are created and driven to propagate in the rock matrix; existing isolated fractures can be connected by the new fractures; the apertures of existing fractures can potentially be reduced or closed due to the changed stress states. An ideal numerical simulator capable of simulating these complex processes needs to properly handle geomechanics, hydrodynamics, complex and arbitrary fracture geometries, and most importantly, their coupling. To this end, we include the following modules in our simulator:

- A solid (geomechanics) solver, providing the non-local mechanical responses of the rock matrix;
- A flow solver, solving the fluid flow in interconnected fracture networks;
- An adaptive remeshing module, generating new meshes for both the solid solver and the flow solver as fractures propagate; and
- A rock joint model, determining hydraulic aperture sizes based on mechanical responses of the rock matrix as well as mechanical responses local to the fracture discontinuities.

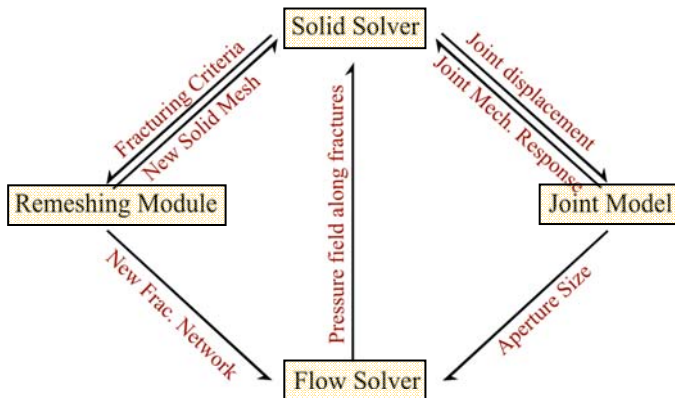


Fig. 1 Important modules of the hydraulic fracturing simulator and information exchange between them in coupled simulations.

In a coupled analysis, these modules share and exchange information with each other as shown in Fig. 1. The key algorithmic aspects of these individual modules are further described in Section 3 of the paper.

We use the Livermore Distinct Element Code (LDEC) as the basic platform, on which our hydraulic fracturing simulator is being developed. LDEC is a 3D computer code developed by the Computational Geosciences Group at LLNL to simulate the response of jointed geologic media to dynamic loading. Additional capabilities, including combined FEM-DEM analysis, fracture mechanics, and explicit solid-fluid coupling have been implemented in LDEC in the continued development over the past decade [9-13]. While LDEC is a rather generic simulation platform, our new development focuses on modules specifically targeting hydraulic fracturing applications, so that we can exploit certain unique features of this process such as small deformation and quasi-static loading, thereby making the simulation computationally more efficient.

3. KEY MODULES

This section describes the algorithmic aspects of the key modules implemented in the hydraulic fracturing simulator.

3.1. FEM Solid Solver

The core of the solid mechanics solver is a conventional explicitly integrated finite element engine utilizing triangular elements. A standard central-difference explicit time integration method is used, so the solver is inherently of a dynamic nature. As will be elaborated on in later sections of the paper, the primary challenge that we face in this study is the high computational cost associated with the coupling of the solid solver and the flow solver. Therefore, some inherent features of the hydraulic fracturing process are exploited to reduce the computational cost, such as using a small deformation formulation and employing a relatively high damping ratio to stabilize the simulations, thanks to the quasi-static nature of this process.

3.2. Solver for Discrete Flow Network

Fluid flow in rock fractures is idealized as laminar flow between two parallel plates. The governing equations are:

$$\frac{\partial q}{\partial l} + \frac{\partial w}{\partial t} = 0 \quad (1)$$

$$\kappa \frac{\partial P}{\partial l} = -q \quad (2)$$

$$\kappa = \frac{w^3}{12\mu} \quad (3)$$

where l and t represent the length along the fracture and time respectively; q is the local flow rate in the fracture at a given cross-section; w is the local aperture size, namely the distance between the two rock walls along the fracture; P is the fluid pressure; and κ represents the

permeability of the fracture, which is a function of the dynamic viscosity μ of the fluid and the local aperture size w . These equations are solved with a modified finite volume method in LDEC. The discrete format of the finite volume method formulation and the boundary conditions to be imposed have been described by Johnson and Morris [11], and are not repeated here. The flow system is solved using a central-difference explicit integration method, which is compatible with the solution method in the solid solver, enabling their efficient coupling.

Despite its simple format, this flow solver adequately models the following two mechanisms important for simulating hydraulic fracturing: 1) flow in fracture networks due to pressure gradient; and 2) the conservation of fluid mass as the total volume of fractures varies (resulting from the creation of new fractures and the varying aperture sizes) with time.

3.3. Time-Stepping Considerations

The critical time step for the flow solver is

$$\Delta t_{flow_crt} = \frac{6\mu}{K} \left(\frac{L_{ij}}{w_{ij}} \right)^2 \quad (4)$$

where L_{ij} is the distance between the centers of two adjacent flow cells i , and j ; w_{ij} is their homogenized average aperture size; and K is the bulk modulus of the fluid. Parameters μ and K are determined by the physical properties of the fluid phase, and L_{ij} can be approximated by the typical lengths of the flow cells, which in turn are determined by the typical element sizes of the solid mesh. The solid solver also has a critical time step size and its value is the smallest mesh length divided by the sound speed in this solid medium. The critical time step for the solid solver is often a few orders of magnitude larger than the flow solver critical time step, and the smaller one of these two dictates a coupled analysis. Meanwhile, the computational cost of each time step for the solid solver is usually much higher than that for the flow solver. Consequently, if the solid solver and the fluid solver are coupled on a step-by-step basis, i.e., they exchange information every time step, the overall computational cost would be unacceptable, since the flow solver determines the total number of time steps (up to billions in a typical simulation) in a simulation and the solid solver determines the cost of each time step.

Our solution to this problem is to employ a “sub-stepping” scheme in the integration, using different step sizes for the two solvers. The time step for the solid solver is N (an integer) times larger than that for the flow solver. The two solvers interchange information after each solid solver time step and N steps in the flow solver. The time-varying aperture at each flow solver step is determined by extrapolation. As both the time step and the deformation of the rock matrix are very small, little

error is induced by extrapolation. The average fluid pressure over the N time steps in the flow solver is fed into the solid solver as stress boundary conditions. This sub-stepping method has been found to greatly reduce the computational cost without impairing simulation accuracy and stability.

3.4. Fracturing Criterion

In the simulator, we use a discrete inter-element cohesive fracture approach similar to the methods proposed by Xu and Needleman [14] and Camacho and Ortiz [15]. In such an approach, a fracturing criterion is specified, and the cohesive elements are invoked where this criterion is met. In typical numerical models dealing with fracture mechanics, very fine meshes are usually used to resolve the stress state at the fracture tip, but this is impractical in our simulations which typically cover a relatively large domain (up to hundreds of meters in each dimension) containing many existing fractures.

Fortunately, the hydraulic fracturing process that we deal with is mostly in the “viscosity-dominated” regime rather than being “toughness-dominated” [16]. The energy dissipated in creating new fracture faces is minimal compared to that consumed by the viscous flow and deformation of the entire rock system driven by the fluid flow. Additionally, the compressive earth stress at typical depths for EGS applications is usually one order of magnitude higher than the tensile strength of most rocks. Therefore, moderate error in predicting the net pressure (fluid pressure in excess of the earth pressure) and energy dissipation required to extending fractures will only have minimal effects on the predicted pumping pressure and pressure distribution over the fracture network. In fact, most of the classic models for hydraulic fracturing assume that as soon as the fluid pressure at the leading edge of a fracture can overcome the compressive earth stress on this plane, the fracture will advance. This argument is supported by a recent study published in Dahi Taleghani’s dissertation [17]. Fracture mechanics is treated relatively rigorously in his study, and he found that viscosity of the fluid dominates the coupled process.

In light of these considerations, we formulate the fracturing criterion simply based on the tensile stress magnitude along potential fracture paths, namely edges between adjacent solid elements. If a threshold value (dependent on properties of the rock, such as strength) is reached, we create new fractures by invoking the adaptive remeshing module, which incorporates the new fractures into the solid mesh and appends new flow cells to the flow network mesh.

3.5. Joint Model

Fractures are treated as mechanical joint elements in the solid solver, and the joint model is a critical component in our simulator. The joint model predicts the local mechanical responses of fractures (opening, closing,

sliding and dilation) to the deformation and stress states in the rock body, and it also provides information regarding the conductivity (i.e. hydraulic aperture sizes) of the fractures to the flow solver. This simulator uses a discrete element-type contact model to handle the interactions between the rock bodies at the two sides along a fracture.

The joint model keeps tracking the locations of the opposing solid elements along a fracture. When they come to contact, a contact stress is applied along the joint, essentially a penalty method. When relative displacement in the tangential direction takes place between these two opposing elements, shear stress is applied and Coulomb's friction law is enforced, making frictional sliding of rocks along the fractures possible. When the two opposing elements separate from each other with a positive distance ($\delta_n > 0$) due to the pressurization of the fracture, the following equation (5) is used to calculate the hydraulic aperture.

$$w = \begin{cases} \delta_n & \text{if } \delta_n > w_r \\ w_r & \text{if } \delta_n \leq w_r \end{cases} \quad (5)$$

where w_r is called the "residual" aperture, which embodies the residual flow conductivity of a closed fracture (i.e. the fluid pressure is not high enough to overcome the compressive rock stress) due to asperity of the fracture surface. Joint models available in the literature of rock mechanics [18] that can more realistically consider mechanical and conductive behaviors of joints are being researched in our study and will be implemented in future models. Nevertheless, the current simple model provides the basic capability to take the most important mechanisms, namely the opening and closing of fractures due to the variation of fluid pressure into account.

4. VERIFYING THE NUMERICAL IMPLEMENTATION AGAINST THE KGD MODEL

4.1. The KGD Model

The so-called KGD model deals with a single fracture driven by a Newtonian fluid at a constant flow rate under the plane-strain assumption as shown in Fig. 2. It was independently developed by Khristianovic and Zheltov [4], and Geertsma and de Klerk [6]. Closed-form solutions are available to predict the length L of the fracture as a function of injection time t if fluid leak-off is ignored. Two solutions are found in the literature shown in equations (6)[17] and (7)[19], with similar formats but slightly different coefficients. The reason for this discrepancy is unknown to the authors.

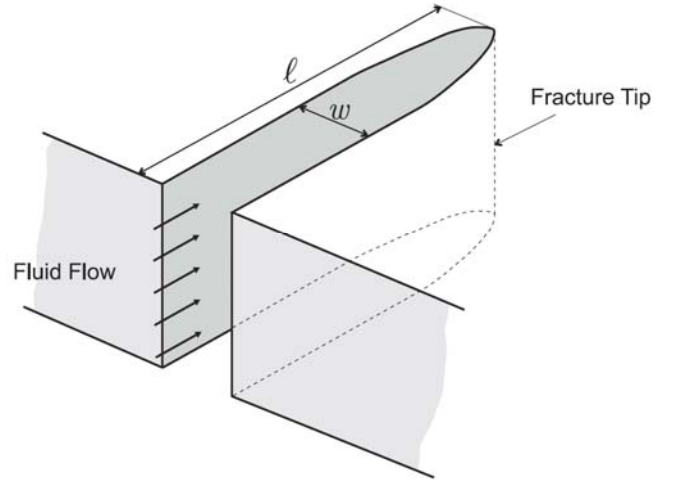


Fig. 2 A schematic illustration of the KGD model (after[3]).

$$l(t) = 0.605 \left[\frac{Gq_0^3}{\mu(1-\nu)} \right]^{\frac{1}{6}} t^{\frac{2}{3}} \quad (6)$$

$$l(t) = 0.679 \left[\frac{Gq_0^3}{\mu(1-\nu)} \right]^{\frac{1}{6}} t^{\frac{2}{3}} \quad (7)$$

where G and ν are the shear modulus and the Poisson's ratio of the rock body; q_0 is the constant injection flow rate per unit thickness along the well bore direction.

4.2. Numerical Model of a KGD Problem

The core simulation domain has dimensions of 100 m and 120 m in the x and y directions, respectively and is discretized into 96,000 triangular elements with uniform sizes. The core mesh is then extended to approximately 1,000 m in each direction with larger elements to reduce the effect of the far field boundaries. "Roller" boundary conditions are applied to all the four edges of the mesh. At the left side boundary this applies a symmetrical condition. Since the KGD model is formulated based on the "net pressure", namely the fluid pressure in excess of the normal stress in the rock acting along the potential fracture direction, no in-situ stress is applied. Other important simulation parameters are listed in Table 1.

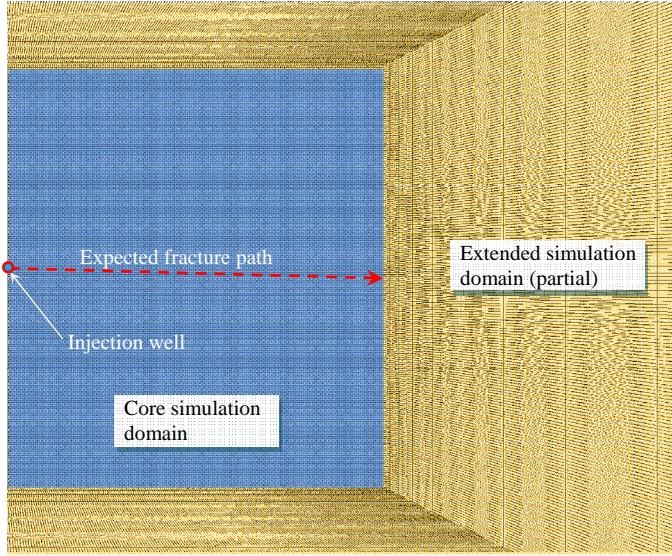


Fig. 3 Mesh of the numerical KGD model.

Table 1 Key model parameters for the KGD simulation

Parameter	Value
Rock, shear modulus G	8 GPa
Rock, Poisson's ratio ν	0.25
Injection rate q_0	10 L per sec. per m thickness
Fluid, dynamic viscosity μ	0.001 Pa·s
Residual aperture size w_r	0.2 mm

4.3. Simulation Results

The comparison of the hydraulic fracture length l as a function of the injection time between the numerical simulation results and the KGD closed-form equations is shown in Fig. 4. The numerical simulation results reasonably match the close-form solutions, especially equation (6). We performed another simulation with two times coarser mesh in each dimension and otherwise identical parameters. The results did not show perceivable change with the variation of the mesh sizes, and thus are not shown in the figure. This observation indicates satisfactory convergence of the model.

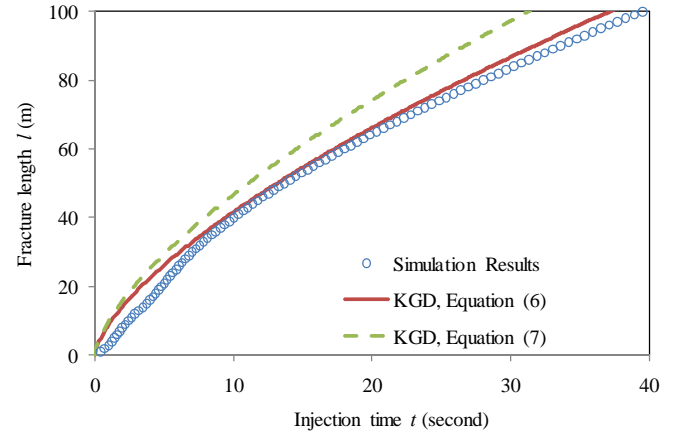


Fig. 4 Length of the hydraulic fracture as a function of the injection time, a comparison between the numerical simulation results and the KGD closed-form equations.

The distributions of fluid pressure P , flow rate q , and aperture size w along the fracture in four selected states during the propagation when the length of the fracture $l=25, 50, 75,$ and 100 m are shown in Fig. 5. During the propagation of the fracture, the majority of pressure drop along the fracture between the injection well and the fracture tip takes place near the tip where the aperture size is much smaller than that near the well bore. The cross-section shape of the fracture is similar to a half-ellipse, meeting the expectation of the KGD model. The flow rate also decreases along the fracture length, reflecting the fluid volume that is consumed by the expansion of the fracture aperture as the fracture propagates, namely the second term in equation (1). The KGD model makes an assumption that the flow rate is constant along the fracture in order to keep the problem analytically tractable. This assumption is apparently not entirely accurate, and our numerical model does not depend on such a simplifying assumption. While the injection flow rate is the flow boundary condition given in the KGD problem, some random fluctuation of the flow rate of q near the injection well when the fracture is short (say $l=25$ m) is noticed in the simulation results. This is because the flow boundary condition in the simulator does not directly control the flow rate. Instead, we use a pressure-controlled boundary condition and a servomechanism to alter the pressure until the desired flow rate is reached. Such fluctuations in the beginning of the simulation are expected and the flow rate converges to the prescribed value as the simulation progresses.

The comparison of the simulation results and the KGD analytical solution demonstrates that our numerical model can effectively handle the coupling between the mechanical responses of solid rock and flow in fractures.

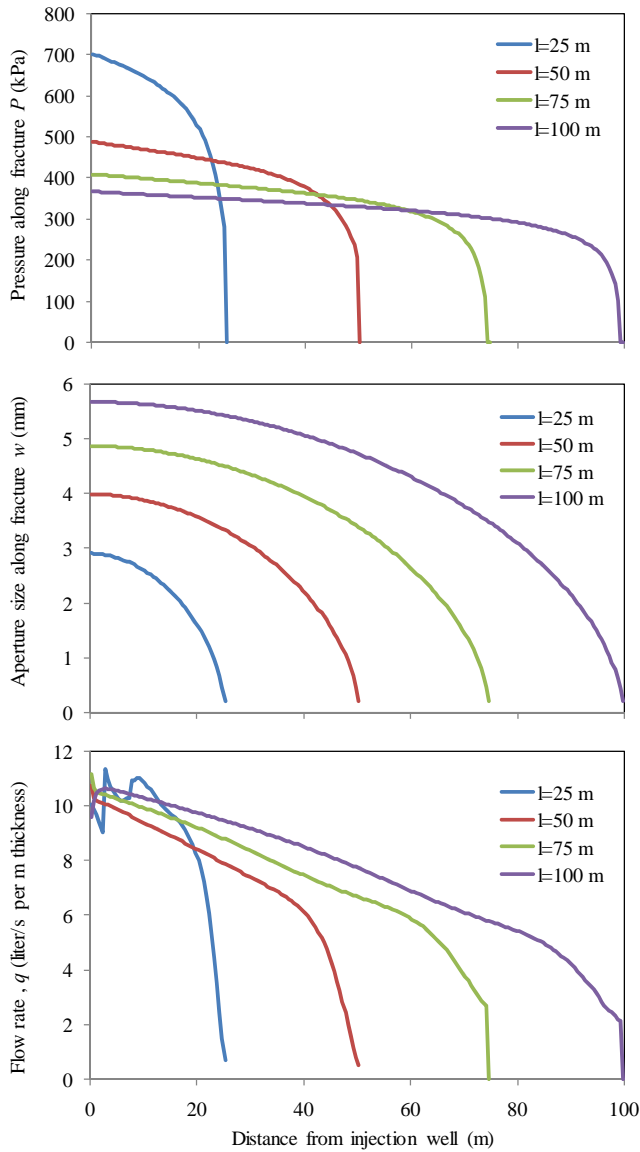


Fig. 5 Distributions of P , w and q along the fracture.

5. SIMULATING OF INTERACTION BETWEEN TWO FRACTURES WITH SIMPLE GEOMETRY

In this section we use the numerical simulator to investigate the interaction between a propagating fracture driven by hydraulic flow and a preexisting fracture. The simulation domain around a short horizontal (along the x axis) fracture and a vertical one (along the y axis) is partially shown in Fig. 6(a). The far field boundary condition is such that homogeneous stress $\sigma_{xx}=-20\text{MPa}$ and $\sigma_{yy}=-10\text{MPa}$ is created if no fracture exists. Fluid injection at a maximum pressure of 18 Pa takes place at the left end of the horizontal fracture, so it is expected to propagate horizontally (the plane with the least compressive stress) and eventually intersects the vertical fracture.

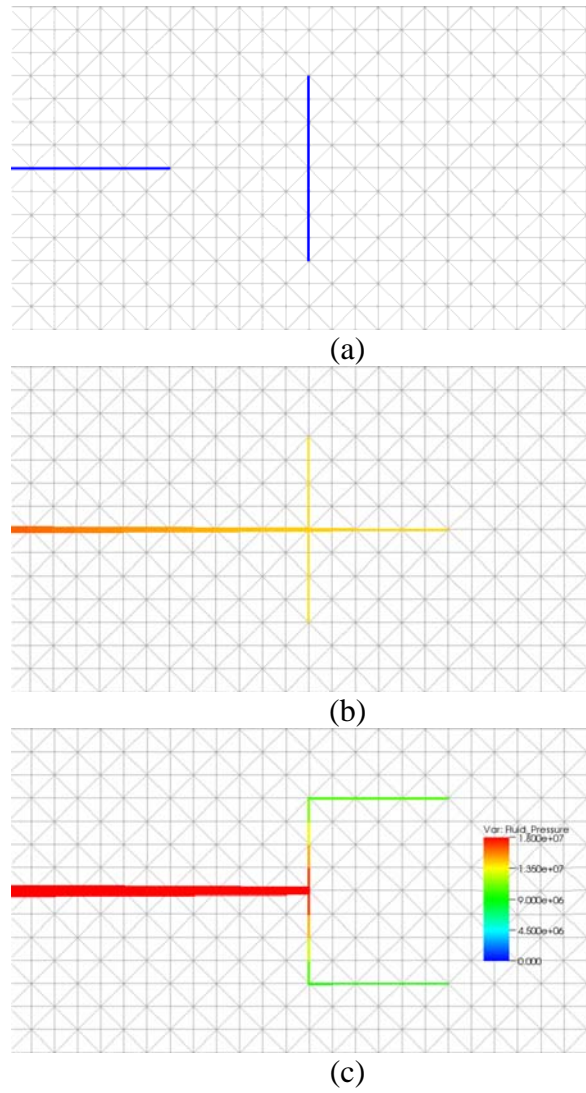


Fig. 6 Interaction between two fractures. (a) The initial configuration; (b) crossing; and (c) offsetting.

The three modes of interaction between such fractures, namely arrest, cross and offset have been extensively studied in the literature [20-22]. It is known that the friction coefficient along the vertical fracture is a key factor determining the mode of interaction. Therefore, we performed two parallel simulations, one assuming a joint friction angle of 45 degrees and the other 3 degrees with otherwise identical parameters, and the simulation results are shown in Fig. 6(b) and (c), respectively. The color in these two figures denotes the fluid pressure along the fracture, and the fracture geometry is magnified in the lateral direction by 20 times to facilitate illustration. The simulation results indicate the interaction mode for the first simulation with 45 degrees of friction angle to be “cross” and the second case being “offset”, as expected according to the analytical solutions available. No further investigation into this problem is elaborated in this paper, but these simulations clearly demonstrate the ability of our numerical model in capturing the essential mechanisms governing the

interactions between fractures driven by pressurized fluid flow.

6. STIMULATING A RELATIVELY COMPLEX PREEXISTING FRACTURE NETWORK AT DIFFERENT LEVELS OF STRESS ANISOTROPY

6.1. Simulation Parameters

In this section we use the hydraulic fracturing simulator to investigate the stimulation of a relatively complex preexisting fracture network at different levels of stress anisotropy.

The simulation domain is 100 m x 100 m, and consisting of 20,000 triangle elements representing the rock matrix. It can be considered as a horizontal cross-section of a reservoir to be stimulated. The rock has a Young's modulus of 20 GPa and a Poisson's ratio of 0.2. The preexisting fracture network is shown in Fig. 7(a), and the injection well is located at $x=0$ m, $y=50$ m, and the production well at $x=100$ m, $y=50$ m. Three parallel simulations (denoted as A, B, and C) are performed, in which the far field deformation-controlled boundary conditions are such that homogeneous stress $\sigma_{yy}=-10$ MPa is created if on fracture exists for all the simulations and σ_{xx} is the variable to be investigated with three levels, -16, -10, and -8 MPa. In fact, the preexisting fractures without pressurized fluid have minimal effects on the stress field due to the presence of the joint model, which applies contact stresses along the fractures. The planes along the x axis have the least compressive stress for simulation A, the stress for simulation B is isotropic, and the planes long the y axis have the least compressive stress for simulation C, which apparently will affect the expected predominant directions of fracture propagation. A fluid with a dynamic viscosity of 0.001 Pa•s is pumped into the fracture system from the injection well at a constant pressure of 16 MPa.

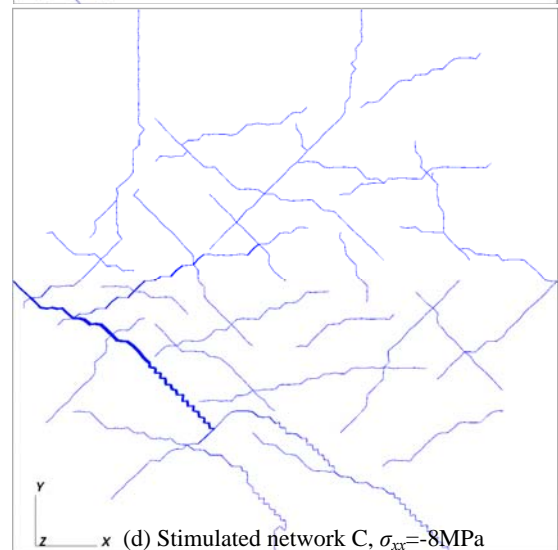
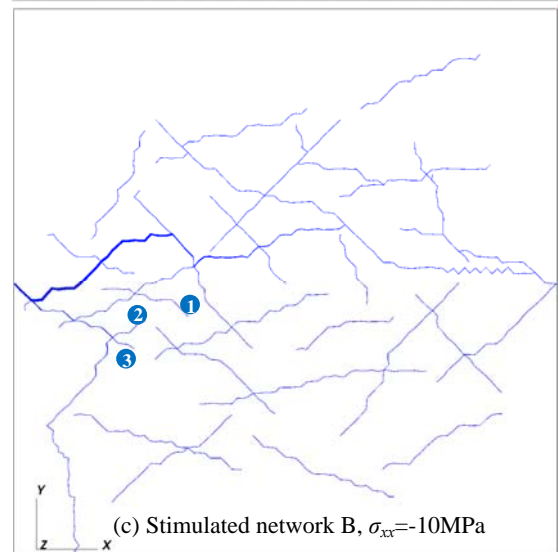
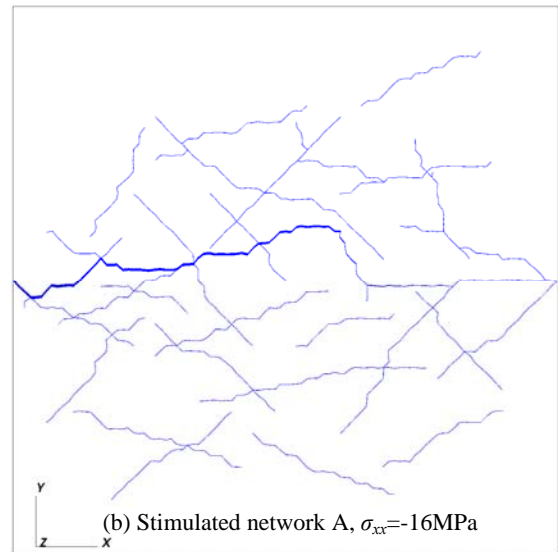
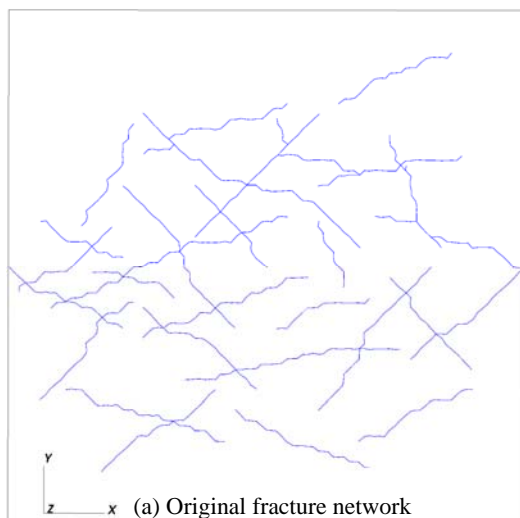


Fig. 7 The original fracture network and the stimulated fracture network at three levels of stress anisotropy.

6.2. Simulation Results

The stimulated networks under the three assumed stress conditions are shown in Fig. 7(b) to (d). In simulation A with the horizontal plane as the least compressive stress

plane and strong stress anisotropy, new fractures are created primarily in the x direction connecting existing branches together and finally reach the production well. In simulation B with isotropic in-situ stress, fractures are stimulated in both the x and y directions. The new fracture running in the y direction near the lower left corner of Fig. 7(c) does not contribute to the conductivity between the injection well and the production well, but it will consume some of the pumping capability and thus serves as a leak-off term in the system, which is undesired. In simulation C, multiple new fractures are created but they all extend primarily in the y direction and do not enhance the conductivity between the injection and production well.

6.3. A Curious Case of Competing Between Fractures

An interesting question to answer is why new fractures do not develop from existing tips near points 1-3 in simulation B as labeled in Fig. 7(c). Fig. 8 shows the stimulated fracture network in the steady state of simulation B with the fluid pressure denoted by the color and height of the vertical “bars”. These three fracture tips are all filled with fluid with relatively high pressure, which potentially can drive these segments of fractures. In order to understand why new fractures are not created here, we need to check the local stress state in this region.

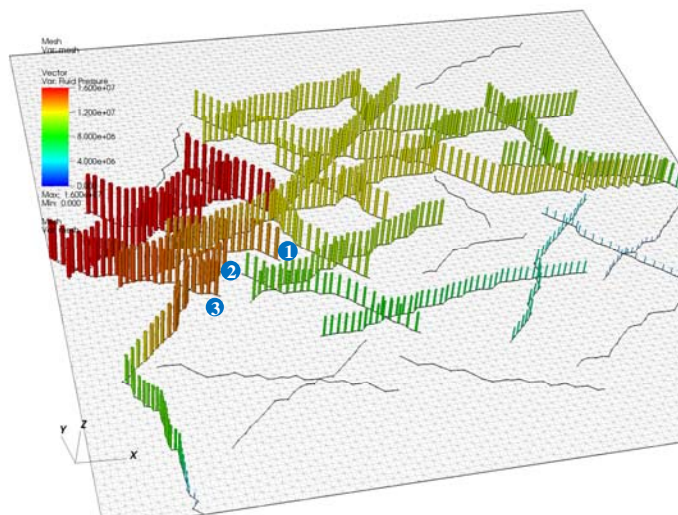
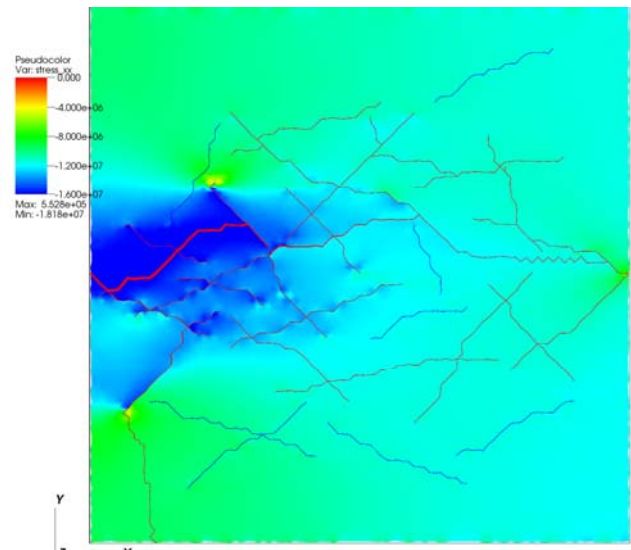
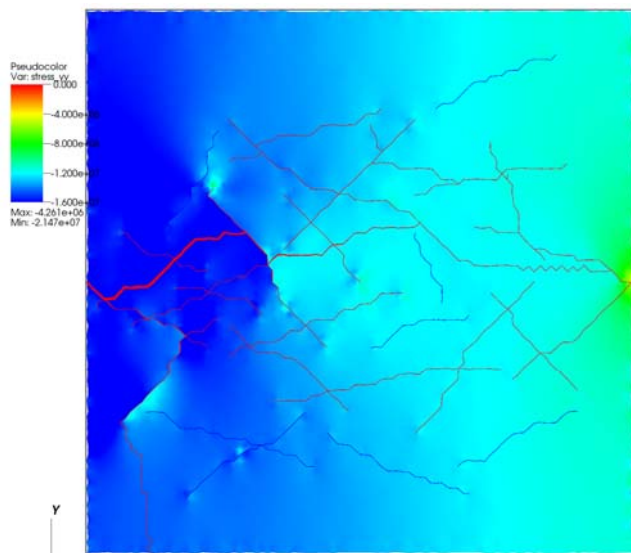


Fig. 8 Fluid pressure distribution over the stimulated fracture network in the steady state of simulation B.

Fig. 9 shows the stress state in the rock matrix. The region near the three fracture tips that we are interested in is largely enclosed by pressurized fractures, which have significantly affected its stress state. Therefore, the compressive stress in this region is close to the fluid pressure, and thus has substantially exceeded the far field stress. This imposes additional constraints to the creation of new fractures and impeded these three particular fracture segments from further extending.



(a)



(b)

Fig. 9 Stress state of the rock matrix: (a) σ_{xx} and (b) σ_{yy} .

The simulation results in section 6.2 regarding the predominant direction of fracture propagation can be considered obvious because they simply reflect the relatively magnitude of the normal stress in the two directions. On the other hand, the analysis in section 6.3 demonstrates the insight that we can obtain from numerical simulations that are not reflected in classical analytical models.

7. CONCLUDING REMARKS

In this paper we present the basic simulation methodology for hydraulic fracturing that is being developed at the Lawrence Livermore National Laboratory. The approach features fully coupled geomechanics and discrete flow network modeling, and has the capability of simulating hydraulic fracturing in a

relatively complex fracture network. The main algorithmic components of the simulator as well as the coupling strategy have been described and three numerical examples are presented. The first example shows that the simulation results reasonably match the prediction of the classical KGD model, thereby verifying the implementation of the solid solver, the flow solver, and most importantly, their coupling. By simulating the interaction between two fractures with simple geometry, the second numerical example demonstrates the ability of the numerical simulator in reflecting the key mechanical mechanisms governing interactions between fractures. Finally, the most important merit of the simulator, namely the ability to handle relatively complex fracture network is demonstrated through the stimulation of a preexisting fracture network under different assumed stress conditions. Currently we are further improving individual modules of the code and validating the simulation results.

Note that the current paper focuses on modeling the interactions between preexisting fractures and new hydraulically driven fractures in relatively complex fracture networks. Quantifying the enhancement of permeability and heat transfer owing to hydraulic fracturing is within the scope of our comprehensive study but beyond the immediate scope of the current paper. Some preliminary results in these regards have been published elsewhere [23].

AUSPICES AND ACKNOWLEDGMENTS

The authors gratefully acknowledge the Geothermal Technologies Program of the US Department of Energy for support of this work under the Enhanced Geothermal Systems Program. The authors also would like to acknowledge their collaborators at the Lawrence Livermore National Laboratory. This work was performed under the auspices of the U.S. Department of Energy by Lawrence Livermore National Laboratory under Contract DE-AC52-07NA27344. This manuscript was approved to be released by LLNL with a release number LLNL-CONF-271641. Neither the United States government nor Lawrence Livermore National Security, LLC, nor any of their employees makes any warranty, expressed or implied, or assumes any legal liability or responsibility for the accuracy, completeness, or usefulness of any information, apparatus, product, or process disclosed, or represents that its use would not infringe privately owned rights. Reference herein to any specific commercial product, process, or service by trade name, trademark, manufacturer, or otherwise does not necessarily constitute or imply its endorsement, recommendation, or favoring by the United States government or Lawrence Livermore National Security, LLC. The views and opinions of authors expressed herein do not necessarily state or reflect those of the

United States government or Lawrence Livermore National Security, LLC, and shall not be used for advertising or product endorsement purposes.

REFERENCES

1. An MIT-led interdisciplinary panel. 2006. *The Future of Geothermal Energy: Impact of Enhanced Geothermal Systems (EGS) on the United States in the 21st Century* (2006).
2. Huttert, K.M., and D.G. Willis. 1957. Mechanics of hydraulic fracturing. *Transactions of The American Institute of Mining And Metallurgical Engineers*, 210: 153-163.
3. Adachi, J., E. Siebrits, A. Peirce, and J. Desroches. 2007. Computer simulation of hydraulic fractures. *International Journal of Rock Mechanics and Mining Sciences*, 44: 739-757.
4. Khristianovic, S.A., and Y.P. Zheltov. 1955. Formation of vertical fractures by means of highly viscous liquid. In *Proceedings of the Fourth World Petroleum Congress*, Rome, 579-86.
5. Perkins, T.K., and L.R. Kern. 1961. Widths of hydraulic fractures. *Journal of Petroleum Technology*, 13: 937-949.
6. Geertsma, J., and F. de Klerk. 1969. A rapid method of predicting width and extent of hydraulically induced fractures. *Journal of Petroleum Technology*, 21: 1,571-1,581.
7. Nordgren, R.P. 1972. Propagation of a vertical hydraulic fracture. *Society of Petroleum Engineers Journal*, 12: 306-314.
8. McClure, M.W., and R.N. Horne. 2010. Discrete fracture modeling of hydraulic stimulation in enhanced geothermal systems. In *Proceedings of the 35th Workshop on Geothermal Reservoir Engineering*, SGP-TR-188, Stanford, California.
9. Morris, J.P., M.B. Rubin, G.I. Block, and M.P. Bonner. 2006. Simulations of fracture and fragmentation of geologic materials using combined FEM/DEM analysis. *International Journal of Impact Engineering*, 33: 463-473.
10. Block, G., M.B. Rubin, J. Morris, and J.G. Berryman. 2007. Simulations of dynamic crack propagation in brittle materials using nodal cohesive forces and continuum damage mechanics in the distinct element code LDEC. *International Journal of Fracture*, 144: 131-147.
11. Johnson, S.M., and J.P. Morris. 2009. Modeling hydraulic fracturing for carbon sequestration applications. In *Proceedings of the 43rd US Rock Mechanics Symposium and the 4th US-Canada Rock Mechanics Symposium*, Asheville, NC, ARMA 09-30.
12. Morris, J.P., and S.M. Johnson. 2009. Dynamic simulations of geological materials using combined FEM/DEM/SPH analysis. *Geomechanics and Geoengineering: An International Journal*, 4: 91-101.

13. Johnson, S.M., and Y. Hao. 2010. Upscaling of thermal transport properties in enhanced geothermal systems. *Fall Meeting of the American Geophysical Union*, San Francisco, CA, Dec. 12-17.
14. Xu, X.P., and A. Needleman. 1994. Numerical simulations of fast crack growth in brittle solids. *Journal of the Mechanics and Physics of Solids*, 42: 1,397-1,434.
15. Camacho, G., and M. Ortiz. 1996. Computational modelling of impact damage in brittle materials. *International Journal of Solids and Structures*, 33: 2,899-2,938.
16. Detournay, E. 2004. Propagation regimes of fluid-driven fractures in impermeable rocks. *International Journal of Geomechanics*, 4: 35-45.
17. Dahi-Taleghani, A. 2009. *Analysis of Hydraulic Fracture Propagation in Fractured Reservoirs : An Improved Model for the Interaction Between Induced and Natural Fractures*. Doctoral dissertation, the University of Texas, Austin.
18. Barton, N., S. Bandis, and K. Bakhtar. 1985. Strength, deformation and conductivity coupling of rock joints. *International Journal of Rock Mechanics and Mining Sciences & Geomechanics Abstracts*, 22: 121-140.
19. Yew, C.H. 1997. *Mechanics of Hydraulic Fracturing*. Gulf Publishing Company, Houston, Texas.
20. Zhang, X., and R.G. Jeffrey. 2006. The role of friction and secondary flaws on deflection and re-initiation of hydraulic fractures at orthogonal pre-existing fractures. *Geophysical Journal International*, 2006; 166(3):1,454-1,465.
21. Thiercelin, M.J. 2009. Hydraulic fracture propagation in discontinuous media. In *Proceedings of the International Conference on Rock Joints and Jointed Rock Masses*. Tucson, Arizona.
22. Gu, H., and X. Weng. 2010. Criterion for fractures crossing frictional interfaces at non-orthogonal angles. In *44th US Rock Mechanics Symposium and 5th U.S.-Canada Rock Mechanics Symposium*. Salt Lake City, Utah.
23. Fu, P., Johnson, S.M., Hao, Y., and Carrigan, C.R. 2011. Fully coupled geomechanics and discrete flow network modeling of hydraulic fracturing for geothermal applications. In *Proceedings of the 36th Stanford Geothermal Workshop*, Stanford, CA, Jan. 31 – Feb. 2, 2011.